


Apparent Kondo effect in Moiré transition metal dichalcogenide bilayers: Heavy fermions versus disorder

Prathyush P. Poduval,^{*} Katharina Laubscher^{✉, *} and Sankar Das Sarma

Condensed Matter Theory Center and Joint Quantum Institute, Department of Physics, University of Maryland, College Park, Maryland 20742, USA

 (Received 31 January 2023; revised 28 June 2023; accepted 28 June 2023; published 3 August 2023)

A recent work by Zhao *et al.* [*Nature (London)* **616**, 61 (2023)] reported the realization of a synthetic Kondo lattice in a gate-tunable Moiré transition metal dichalcogenide bilayer system. The observation of a Kondo lattice is supported by a plateau (or dip, depending on filling) in the temperature dependence of the resistivity $\rho(T)$ around $T^* \sim 40$ K, which is interpreted as the Kondo temperature scale, and an apparent enhancement of carrier mass extracted from the low-temperature resistivity data, indicating the emergence of “heavy fermions.” The latter observation is crucially based on the assumption that the primary resistive scattering mechanism is electron-electron scattering in the underlying Fermi liquid. In this work, we analyze the experimental data under the assumption that the primary resistive scattering mechanism is *not* electron-electron scattering, but Coulomb scattering by random quenched charged impurities and phonon scattering. We show that a combination of impurity and phonon scattering is a plausible alternative explanation for the observed resistivity that can describe the key features of the experimental data, even if no Kondo lattice has formed, indicating that further theoretical and experimental work is needed to conclusively verify the formation of a Kondo lattice in the work by Zhao *et al.*

DOI: [10.1103/PhysRevB.108.085405](https://doi.org/10.1103/PhysRevB.108.085405)

I. INTRODUCTION

The possibility of realizing a synthetic Kondo lattice and heavy fermions in multilayer Moiré materials has attracted significant interest over the past few years [1–11]. Following recent theoretical proposals, an important experimental work [1] reported the observation of a Kondo lattice in a hole-doped MoTe₂/WSe₂ Moiré transition metal dichalcogenide (TMD) heterobilayer system. Here, the MoTe₂ layer is brought into a Mott-insulating state hosting localized magnetic moments, while the WSe₂ layer provides essentially free itinerant holes that couple to the localized spins via the Kondo exchange coupling. Based on an assumed interplay of these ingredients, Ref. [1] inferred the realization of a Kondo lattice when the Fermi level is tuned inside the Mott gap of the MoTe₂ layer. The experimental characteristic features of the purported Kondo lattice were probed indirectly by temperature-dependent resistivity measurements in Ref. [1]: First, under the assumption that electron-electron scattering of the underlying Fermi liquid is the main resistive scattering mechanism, the effective quasiparticle mass is extracted by fitting a quadratic function to the low-temperature resistivity-vs-temperature data [12]. This yields a large value of $m \simeq 5 - 10m_e$ (here, m_e is the bare electron mass) in the region of the phase diagram where the Kondo lattice is expected. Indeed, such a mass would be consistent with a Kondo lattice, where the strong Kondo exchange coupling leads to the emergence of quasiparticles with a large effective mass

(“heavy fermions”) [13,14]. Second, beyond a certain characteristic temperature $T^* \sim 40$ K, the resistivity-vs-temperature curve starts to flatten out or even decrease with temperature. In Ref. [1], this characteristic temperature was interpreted as the Kondo temperature.

The Kondo physics interpretation in Ref. [1] is based entirely on the low-temperature resistivity measurement being interpreted as arising from electron-electron scattering, with other resistive scattering mechanisms assumed to be negligible. Previous studies, however, showed that even non-Kondo two-dimensional (2D) electron gases may, under suitable conditions, manifest a rich and nonmonotonic temperature dependence of the resistivity due to an interplay of different competing scattering mechanisms that become operational in different temperature regimes. In 2D semiconductors, including possibly 2D Moiré TMDs, screened disorder scattering [15–21] typically leads to a resistivity that increases linearly with temperature for $T \ll T_F$, where T_F is the Fermi temperature. At higher temperatures, the system undergoes a quantum-to-classical crossover from the strongly screened quantum regime at $T \ll T_F$ to the classical regime at $T > T_F$, where the resistivity now decreases as $1/T$. At the same time, at high temperatures $T > T_{BG}$, where T_{BG} is the Bloch-Grüneisen temperature, an additional linear-in- T contribution to the resistivity due to electron-phonon scattering becomes relevant [22,23]. Depending on the relative magnitudes of T_{BG} and T_F , different dependences of the resistivity on temperature are possible, arising simply from the interplay of impurity scattering and phonon scattering. In particular, when $T_{BG} > T_F$, a flattening or even a local minimum of the resistivity may arise in the intermediate-temperature regime

^{*}These authors contributed equally to this work.

($T \sim T^*$), with the behavior being a linear-in- T increase (from impurity scattering) below T_F and a linear-in- T increase (from phonon scattering) for $T > T_{BG}$. This can give rise to resistivity-vs-temperature behavior manifesting the same qualitative features observed in the resistivity data of Ref. [1]. Therefore, we believe that an analysis based on just the temperature-dependent resistivity data is not sufficient to conclusively identify the onset of a Kondo lattice phase since the possibility that the resistivity is controlled by impurity and phonon scattering rather than electron-electron scattering cannot be ruled out.

To show that an explanation based on disorder and phonon scattering is compatible with the resistivity data reported in Ref. [1], we first present empirical fits to the experimental data, taking into account the different scattering mechanisms discussed above. We show that the transport signatures reported in Ref. [1] can be qualitatively explained by a combination of screened disorder scattering (governing the low- to intermediate-temperature regime) and electron-phonon scattering (dominant in the high-temperature regime). While we also provide the physical parameters extracted from our fits, these should be viewed as crude qualitative estimates at best, rather than quantitatively exact numbers, since the uncertainties associated with the experimental data are considerable, particularly with regard to the true carrier density, the disorder configuration, and the residual $T = 0$ resistivity at various electric fields; in fact, the resistivity data at low temperatures have substantial unexplained variations, making a precise quantitative extraction of the underlying parameters impossible [25]. Based on our analysis, we conclude that a combination of disorder and phonon scattering provides a reasonable explanation for the reported temperature-dependent resistivity data and that additional experimental signatures are required to conclusively verify the observation of a Kondo lattice. Our work shows that impurity and phonon scattering together can explain the temperature-dependent resistivity of Ref. [1] without resorting to electron-electron scattering effects at all.

II. MODEL AND SCATTERING MECHANISMS

Reference [1] discusses a MoTe₂/WSe₂ Moiré TMD system with hole doping, where the MoTe₂ layer is an insulator while the holes in the WSe₂ layer are itinerant. To analyze the resistivity of the Moiré system, we consider transport by 2D carriers modeled by a parabolic dispersion $\epsilon_k = \hbar^2 k^2 / 2m$. Here, \mathbf{k} is the 2D wave vector, and m is the effective mass of the itinerant holes. Since the WSe₂ layer does not feel the Moiré potential, the corresponding band can be approximated by a parabolic dispersion [1,25]. The effective parameters of this parabolic dispersion (the mass m and Fermi temperature T_F) can, however, be renormalized by interactions between the carriers of the WSe₂ layer and the localized states of the MoTe₂ layer. Throughout this work, we take the effective mass m and the Fermi temperature T_F as free parameters which we fit to the experimental data (see below). The system is further characterized by the 2D carrier density n , the background lattice dielectric constant κ (which we take to be $\kappa = 10$), and the total (spin) degeneracy $g = 2$. The resistivity

is given by the Drude formula

$$\rho(T) = \frac{m}{ne^2\tau(T)}, \quad (1)$$

where $\tau(T)$ is the finite-temperature transport scattering time. In our work, we consider three possible contributions to the finite-temperature scattering: (1) Coulomb scattering mediated by charged disorder arising from random quenched impurities, (2) electron-electron scattering, and (3) electron-phonon scattering.

We start by discussing disorder scattering, which is present even at $T = 0$, producing a substantial residual resistivity in the data of Ref. [1]. Assuming that the carriers scatter only within the 2D plane of the Moiré system [26], the 2D Coulomb interaction is given by $V_q = \frac{2\pi e^2}{\kappa q}$, which corresponds to the 2D Fourier transform of the three-dimensional (3D) Coulomb potential. The bare Coulomb potential of the charged disorder is screened by the carriers themselves, resulting in the screened potential

$$u_q = \frac{V_q}{\epsilon(q, T)} = \frac{2\pi e^2}{\epsilon(q, T)\kappa q}, \quad (2)$$

where, within the random-phase approximation (RPA) screening theory, $\epsilon(q, T)$ is the finite-temperature static RPA screening function in two dimensions, given by

$$\epsilon(q, T) = 1 + \frac{2\pi e^2}{\kappa q} \Pi(q, T). \quad (3)$$

Here, $\Pi(q, T)$ is the 2D finite-temperature static polarizability function. At $T = 0$, the polarizability function is given by [27]

$$\Pi(q, T = 0) = N_F [1 - \sqrt{1 - (2k_F/q)^2} \Theta(q - 2k_F)], \quad (4)$$

where $N_F = gm/2\pi\hbar^2$ is the 2D density of states, with $g = 2$ being the total degeneracy (spin); k_F is the Fermi momentum; and $\Theta(x)$ is the Heaviside step function. At $T = 0$, the disorder scattering occurs on the Fermi surface. As a result, the maximum value of q is given by $0 \leq q \leq 2k_F$, with $2k_F$ scattering being the dominant resistive scattering process. Within this regime, the polarizability function is constant, and the screening function is s -wave. The finite-temperature polarizability function can be calculated using the corresponding $T = 0$ function via [18,28,29]

$$\Pi(q, T) = \frac{\beta}{4} \int_0^\infty d\mu' \frac{\Pi(q, T = 0)|_{\epsilon_F = \mu'}}{\cosh^2 \frac{\beta}{2}(\mu - \mu')}, \quad (5)$$

where $\beta = 1/k_B T$, ϵ_F is the Fermi energy, and μ is the finite-temperature chemical potential, given by

$$\mu(T) = k_B T \ln \left[\exp\left(\frac{T_F}{T}\right) - 1 \right]. \quad (6)$$

The primary effect of finite temperature is to smoothen the kink of the polarizability function at $q = 2k_F$. This thermal smoothening of the $2k_F$ kink has a nonanalytic form in two dimensions, leading to a strong suppression of screening and hence to strong temperature dependence of the resistivity arising from impurity scattering in two dimensions which does not happen in 3D systems. This 2D Fermi surface anomaly leads to linear-in- T Fermi liquid corrections to various properties, including the resistivity, rather than the generic

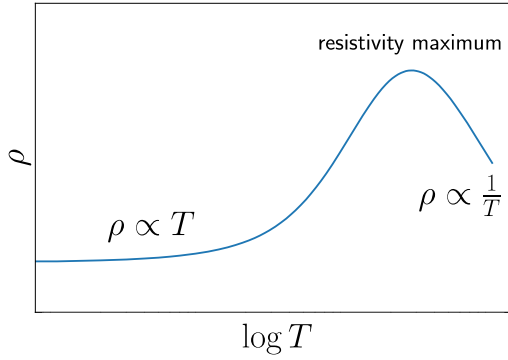


FIG. 1. Schematic dependence of resistivity on temperature as expected from scattering by random charged Coulomb disorder. We point out the existence of a resistivity maximum, which can resemble the resistivity peak in a Kondo lattice [24].

$O(T^2)$ leading order corrections expected from the Sommerfeld expansion. One can think of the anomalous resistive scattering as arising from the strongly temperature dependent 2D Friedel oscillations associated with the impurity screening [30].

The transport scattering time from charged disorder at energy $\epsilon_k = \hbar^2 k^2 / 2m$ is given by [31]

$$\frac{1}{\tau(\epsilon_k)} = \frac{2\pi n_i}{\hbar} \int_{k'} \frac{d^2 k'}{(2\pi)^2} |u_{k-k'}|^2 (1 - \cos \theta_{k'k}) \delta(\epsilon_{k'} - \epsilon_k), \quad (7)$$

where n_i is the charged impurity density, $\theta_{k'k}$ is the angle between \mathbf{k} and \mathbf{k}' , and u_q is the screened Coulomb interaction [see Eq. (2)]. At finite temperatures, the scattering time is calculated in the Boltzmann transport theory by averaging over all energies via

$$\tau(T) = \frac{\int d\epsilon \epsilon \tau(\epsilon) \left(-\frac{\partial f}{\partial \epsilon}\right)}{\int d\epsilon \epsilon \left(-\frac{\partial f}{\partial \epsilon}\right)}, \quad (8)$$

where $f(\epsilon) = 1 / [\exp(\frac{\epsilon - \mu}{k_B T}) + 1]$ is the Fermi distribution function. Using this expression for $\tau(T)$, we can asymptotically expand $\rho(T)$ in the two opposite limits of low temperatures ($T \ll T_F$) and high temperatures ($T \gg T_F$), which gives [17–19]

$$\rho(T \ll T_F) = \rho_0 \left(1 + \frac{2q_s}{q_s + 1} \frac{T}{T_F}\right), \quad (9)$$

$$\rho(T \gg T_F) = \rho_1 \frac{T_F}{T}, \quad (10)$$

where $q_s = q_{TF} / 2k_F$, with $q_{TF} = \frac{gme^2}{\kappa \hbar^2}$ being the 2D Thomas-Fermi screening wave vector; ρ_0 is the residual resistivity at $T = 0$; and $\rho_1 = (h/e^2)(n_i/n)(\pi q_s^2/2)$. We note that at low T , the resistivity rises linearly in T from the $T = 0$ residual resistivity value, and at high T , the impurity induced resistivity decreases as $1/T$, implying an impurity scattering induced resistivity maximum around $T \sim T_F$. This is illustrated in Fig. 1, which schematically shows $\rho(T)$ resulting from scattering by random charged impurities. Between the two limiting regimes $T \ll T_F$ and $T \gg T_F$, there is a crossover regime featuring

a resistivity maximum, which can mimic the characteristic resistivity maximum that arises in a Kondo lattice at $T \sim T_K$.

At very low temperatures, the temperature dependence of the resistivity is additionally suppressed due to the impurity scattering induced broadening of the Fermi surface. The resulting temperature dependence approximately follows [19,32]

$$\rho(T) \simeq \rho_0 [1 + aT \exp(-T_D/T)], \quad (11)$$

where $a = \frac{2q_s}{q_s + 1}$ and T_D is the Dingle temperature defined by $T_D = \hbar / 2k_B \tau_q$, where τ_q is the single-particle relaxation time. The single-particle relaxation time is simply the imaginary part of the self-energy of the electron, which is

$$\frac{1}{\tau_q} = \frac{2\pi n_i}{\hbar} \int_{k'} \frac{d^2 k'}{(2\pi)^2} |u_{k-k'}|^2 \delta(\epsilon_{k'} - \epsilon_k). \quad (12)$$

The above expression differs from the transport scattering time [Eq. (7)] by the $(1 - \cos \theta)$ vertex correction factor that prefers backscattering ($\theta \sim \pi$) over forward scattering ($\theta \sim 0$).

Next, we discuss electron-electron scattering. This manifestly temperature-dependent scattering mechanism is dominant in a clean Fermi liquid, in which the electrons scatter among themselves through the interelectron Coulomb interaction. This leads to a finite lifetime of the electrons, the exact form of which depends on the details of the material and the microscopic model used. We will assume a scattering rate of the form arising in the standard 2D Fermi liquid theory [33–36]

$$\frac{1}{\tau(T)} \simeq \frac{\pi \epsilon_F}{4\hbar} \left(\frac{k_B T}{\epsilon_F}\right)^2, \quad (13)$$

which is valid in the limit $T \ll T_F$. This leads to, assuming electron-electron scattering, a temperature-dependent resistivity of the form

$$\rho(T \ll T_F) = \rho_0 + \frac{\pi^2 \hbar}{2} \frac{T}{e^2} \left(\frac{T}{T_F}\right)^2, \quad (14)$$

where ρ_0 is the $T = 0$ residual resistivity caused by disorder scattering. Note that the electron-electron scattering by itself cannot produce a $T = 0$ residual resistivity, which is clearly observed in Ref. [1], indicating the presence of considerable disorder scattering. Writing Eq. (14) as $\rho(T) = \rho_0 + AT^2$, Ref. [1] uses the quadratic coefficient A to estimate the effective band mass since $\sqrt{A} \sim 1/T_F \sim m$, assuming a known carrier density.

Finally, we discuss the contribution of phonon scattering to the resistivity, which also operates only at finite temperatures and is negligible for $T \ll T_{BG}$, where T_{BG} is the Bloch-Grüneisen temperature. (We mention that in normal metals, T_{BG} is much larger than the Debye temperature T_{Debye} , and hence, T_{Debye} is the lower cutoff temperature scale for phonon scattering, but in doped semiconductors, such as TMDs, $T_{BG} \ll T_{Debye}$, and hence, T_{BG} is the lower cutoff scale for phonon scattering.) For the Moiré systems under consideration, the Bloch-Grüneisen temperature follows $T_{BG} \sim 20\sqrt{n}/10^{12} \text{ cm}^{-2} \text{ K}$, where n is in units of cm^{-2} [37]. At temperatures above T_{BG} , the phonon contribution to the resistivity

is linear in T and is given by [22,23]

$$\rho_{\text{ph}}(T \gg T_{\text{BG}}) = \rho_0 + A_{\text{ph}}T, \quad (15)$$

where the slope A_{ph} is related to the dimensionless parameter λ that characterizes the electron-phonon coupling strength [23]:

$$A_{\text{ph}} = \frac{m}{ne^2} (2\pi\lambda) \frac{k_B}{\hbar}, \quad (16)$$

where $\lambda \sim 0.05$ for TMD materials [37,38]. We are using an approximate estimated value of the electron-phonon coupling for TMDs combining both the deformation potential and piezoelectric interactions. Below T_{BG} , the phonon contribution to $\rho(T)$ is heavily suppressed and goes as $\sim T^4$:

$$\rho_{\text{ph}}(T \ll T_{\text{BG}}) = \rho_0 + B_{\text{ph}} \left(\frac{T}{T_{\text{BG}}} \right)^4. \quad (17)$$

In our analysis, we will assume the functional form of the phonon resistivity contribution is

$$\rho_{\text{ph}}(T) = A_{\text{ph}}(T - T_{\text{BG}})\Theta(T - T_{\text{BG}}), \quad (18)$$

neglecting the phonon contribution below T_{BG} , assuming that the corresponding $O((T/T_{\text{BG}})^4)$ contribution to $\rho_{\text{ph}}(T)$ is negligible (which is true).

III. LOW-TEMPERATURE BEHAVIOR: T VERSUS T^2

In Ref. [1], experimental data for $\rho(T)$ was presented at different filling factors $\nu = 1 + x$ and $\nu = 2 + x$ written in terms of the independent filling factors of the two layers $\nu = \nu_{\text{Mo}} + \nu_{\text{W}}$. Based on the scattering models introduced above, we now provide qualitative fits to the experimental data and discuss the relative importance of the different scattering mechanisms in different temperature regimes. Throughout this paper, we mainly focus on the case $\nu = 1 + x$ and only briefly comment on the case of $\nu = 2 + x$ at the end. This is consistent with the emphasis in Ref. [1].

The first question we consider is whether the mechanism responsible for the low-temperature variation of resistivity is primarily electron-electron scattering or Coulomb disorder scattering. Note that, by definition, disorder scattering is important at the lowest temperatures since it contributes to the residual resistivity ρ_0 , with a leading order linear-in- T correction, and the electron-electron scattering vanishes at the lowest temperatures and is quadratic in temperature. The distinguishing factor is clear: For $T \ll T_F$, the electron-electron scattering contribution to the resistivity depends quadratically on temperature, $\rho = \rho_0 + AT^2$, with the coefficient $A > 0$, while the disorder scattering contribution follows a linear dependence, $\rho = \rho_0(1 + BT)$, with the coefficient $B > 0$. In Fig. 2, we directly compare a linear fit [Fig. 2(a)] with a quadratic fit [Fig. 2(b)] with respect to the experimentally measured $\rho(T)$ in Ref. [1] at filling $\nu = 1 + x$. We find that the linear fit is generally better than the quadratic one, signifying that disorder scattering by itself is a plausible explanation for the observed low-temperature resistivity. Of course, in reality, both scattering mechanisms may be present simultaneously. However, we do not fit a combination of a linear function and a quadratic function since we are interested in studying only the *dominant* scattering mechanism and want to

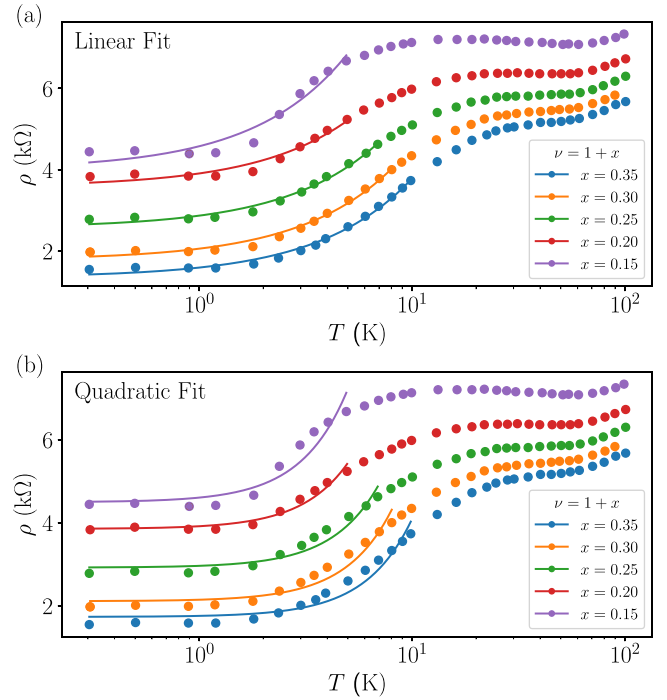


FIG. 2. Fits (solid lines) to the low-temperature experimental resistivity data $\rho(T)$ taken from Ref. [1] (dots) at filling $\nu = 1 + x$. (a) Linear fit (disorder scattering) and (b) quadratic fit (electron-electron scattering). We find that the linear fit is in better agreement with the experimental data than the quadratic fit, signifying the importance of disorder scattering at low temperatures.

keep the number of fitting parameters to a minimum. (Also, the data in Fig. 2 are simply not accurate enough for theoretical fits to multiple combined power laws in temperature.) We note that, even though Eq. (9) is, strictly speaking, valid for only $T \ll T_F$, we perform the fit up to $T \sim 10$ K since the experimentally measured resistivity follows the linear trend very well in this regime. Moreover, at very low temperatures, it is difficult to meaningfully distinguish the linear and quadratic fits due to the small number of experimental data points.

Next, we extract the relevant physical parameters from the best fits shown in Fig. 2. In the case of disorder scattering, we use Eq. (9) together with the relations $q_s(T_F, m) = \frac{ge^2}{2\kappa\hbar} \sqrt{\frac{m}{2k_B T_F}}$ and $m(T_F) = \frac{2\pi n \hbar^2}{g k_B T_F}$ to relate the linear coefficient B to the Fermi temperature T_F while keeping the density n fixed. We consider two scenarios, $n = xn_M$ and $n = (1 + x)n_M$, where $n_M \simeq 5 \times 10^{12} \text{ cm}^{-2}$ is the Moiré density reported in Ref. [1]. The former scenario is what is expected for a doped Mott insulator, while the latter scenario is the carrier density determined from experimental Hall measurements [1]. The resulting values for T_F and m are shown in Table I. We find that the Fermi temperatures extracted from the fit are consistent with experimental estimates [39], while the band mass is larger than the mass $m = 0.5m_e$ expected for itinerant holes in WSe_2 , which we attribute to the uncertainties in the experimental carrier density and residual $T = 0$ resistivity [39]. Due to these significant uncertainties, we also find that the mass extracted

TABLE I. Fermi temperature T_F and effective mass m as extracted from the linear fit (disorder scattering) to the experimental resistivity data of Ref. [1] at filling $\nu = 1 + x$. Values with subscript 1 (subscript 2) are obtained using $n = xn_M$ [$n = (1 + x)n_M$].

x	$T_F _1$ (K)	$m/m_e _1$	$T_F _2$ (K)	$m/m_e _2$
0.35	10.7	4.5	10.9	17.5
0.30	12.4	3.4	12.7	14.6
0.25	16.0	2.2	16.5	10.9
0.20	21.5	1.3	22.7	7.8
0.15	12.6	1.6	13.1	12.7

from the fits varies between different fillings, while it should remain constant in an ideal scenario. We note that the band mass is enhanced in the case of $n = (1 + x)n_M$ by about a factor of 5–10 with respect to the $n = xn_M$ case since the carrier density increases by a factor of 5–10. In order to keep T_F the same (which is a function of n/m), the band mass needs to scale with the carrier density.

We also extract the physical parameters from the quadratic fit assuming that electron-electron scattering is the primary scattering mechanism. Using Eq. (14), we relate the fitting coefficient A to the Fermi temperature T_F . The band mass is then found as a function of T_F and n , which we again assume to be fixed to either $n = xn_M$ or $n = (1 + x)n_M$. Our results are summarized in Table II. Again, we find that the Fermi temperatures extracted from the fit are consistent with experimental estimates [39], while the band masses, in the case of $n = (1 + x)n_M$, are about a factor of 10–20 larger than the mass $m = 0.5m_e$ expected for itinerant holes in WSe₂.

In a typical Kondo lattice, we expect the $T = 0$ resistivity to remain approximately constant as we vary the carrier density [24], which is not observed in the experimental data of Ref. [1], where the $T = 0$ resistivity increases drastically as the carrier density is decreased. Moreover, the resistivity peaks in the experimental data are not very pronounced and correspond more to a flattening of the resistivity curves. These observations point to the existence of a classic metal-insulator transition (MIT) driven by charged Coulomb disorder, which has, indeed, been observed at around $x \sim 0.05$ in the same sample [39]. In this spirit, we calculate the Anderson localization critical density (for $x < 0.35$) defined by the

TABLE II. Fermi temperature T_F and effective mass m as extracted from the quadratic fit (electron-electron scattering) to the experimental resistivity data of Ref. [1] at filling $\nu = 1 + x$. Values with subscript 1 (subscript 2) are obtained using $n = xn_M$ [$n = (1 + x)n_M$]. Note that in this model, T_F is independent of n .

x	T_F (K)	$m/m_e _1$	$m/m_e _2$
0.35	29.4	1.7	6.3
0.30	26.1	1.6	6.9
0.25	22.3	1.6	7.8
0.20	22.3	1.2	7.4
0.15	11.2	1.9	14.3

Ioffe-Regel-Mott criterion [40],

$$\epsilon_F \tau = 1, \quad (19)$$

assuming an impurity density of $n_i \sim 10^9 \text{ cm}^{-2}$ (as extracted from the $T = 0$ resistivity at $\nu = 1 + 0.35$). We find that the localization critical density is about $x \sim 0.01$ – 0.02 , which is consistent with the MIT observed in unpublished data [39] associated with Ref. [1]. In fact, very recent unpublished data [25] from the Cornell group taken on a new sample, which is dirtier, explicitly showed a doping-driven metal-insulator transition at $\nu = 1 + 0.05$ by going to millikelvin temperatures, which is again consistent with our theory since we can estimate the impurity content of this new sample (from the low- T resistivity itself) to be $n_i \sim 2 \times 10^9 \text{ cm}^{-2}$. The observation of the doping induced metal-insulator transition is completely inconsistent with a Kondo lattice interpretation of the experimental transport data and is completely consistent with our interpretation based on disorder scattering being the dominant $T = 0$ scattering mechanism. Note that it was already emphasized in Ref. [21] that doped homobilayer TMDs undergo a low-doping Anderson-type metal-insulator localization transition induced by Coulomb disorder, and our current work shows the same to be true for the heterobilayer TMDs of Ref. [1]—both arise from the presence of strong Coulomb disorder in TMD samples with the low- T mobility being only around a few thousand square centimeters per volt second, indicating the presence of substantial ($\sim 10^{11} \text{ cm}^{-2}$) charged impurities in the environment, as reflected in the rather large residual resistivity.

IV. HIGH-TEMPERATURE BEHAVIOR

We now proceed to study the high- T behavior of $\rho(T)$ using a combination of qualitative fits and exact theory. Figure 3 shows a fit to the full experimental resistivity data at filling $\nu = 1 + 0.35$. Here, we proceed in three steps: First, we perform a linear fit $\rho(T) = \rho_0(1 + BT)$ to the low-temperature data for ρ_0 and B , taking disorder scattering to be the dominant scattering mechanism in this regime [Fig. 3(a)]. This is the same fit as the one shown in Fig. 2(a). Second, at high temperatures, the linear $\rho(T) \sim T$ dependence from disorder scattering undergoes a smooth crossover to $\rho(T) \sim 1/T$ [see Eq. (10)]. To capture this crossover, we perform an additional fit to the high-temperature resistivity data using a fitting function of the form

$$\rho(T) = \rho_0[1 + BT \exp(-T/T_0)] + \frac{C}{T}, \quad (20)$$

where T_0 and C are the fitting parameters and ρ_0 and B are fixed to the values obtained from the low-temperature fit discussed above. Here, the factor of $\exp(-T/T_0)$ is a phenomenological way of suppressing the linear-in- T behavior (valid for $T \ll T_F$) and capturing the smooth quantum-classical crossover to $\rho(T) \sim 1/T$ (for $T \gg T_F$). The resulting curve is shown in Fig. 3(b). Third, this is not a very good fit since we need another ingredient: the linear-in- T phonon scattering that sets in at high temperatures $T > T_{BG}$.

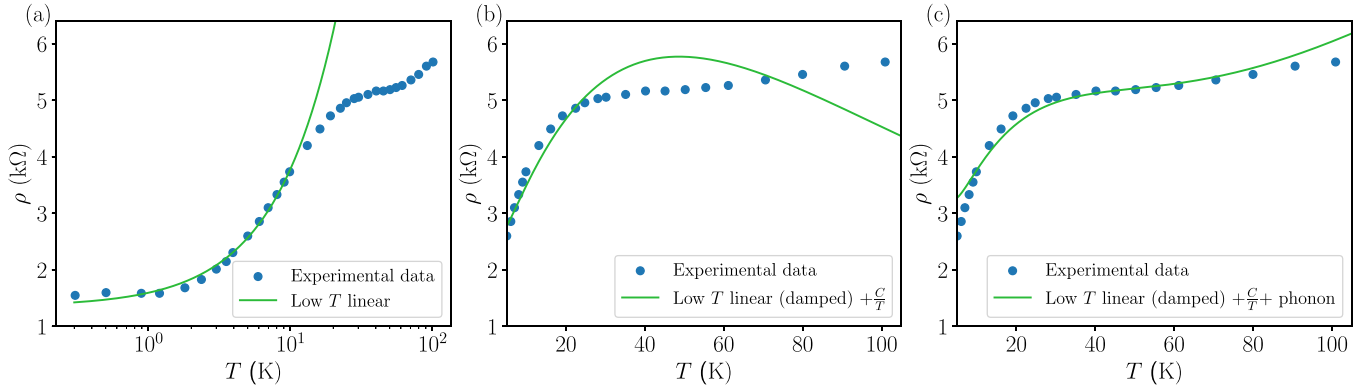


FIG. 3. Fits to the experimentally measured resistivity $\rho(T)$ at filling $\nu = 1 + 0.35$, taken from Ref. [1], assuming screened disorder scattering and electron-phonon scattering as the primary scattering mechanisms. (a) Linear fit in the low-temperature regime, including only disorder scattering [same as in Fig. 2(a)]. (b) Combined fit capturing the crossover of the disorder contribution from $\rho(T) \sim T$ at $T \ll T_F$ to $\rho(T) \sim 1/T$ at $T \gg T_F$ [see Eq. (20)]. (c) Fit including the contribution of disorder scattering to the resistivity [as in (b)] with an additional linear-in- T contribution from phonon scattering [see Eq. (21)], which reproduces the experimental data reasonably well.

Therefore, assuming that Matthiessen's rule is valid within the temperature regime we consider, we add a term given by $A_{\text{ph}}T$, with $\lambda = 0.05$. We recalculate the fit for C and T_0 using the functional form

$$\rho(T) = \rho_0[1 + BT \exp(-T/T_0)] + \frac{C}{T} + A_{\text{ph}}T \quad (21)$$

to obtain the curve in Fig. 3(c), which is now in good agreement with the experimental data. Thus, disorder scattering (including quantum-classical crossover and Friedel oscillation effects) plus phonon scattering provides an acceptable explanation for the temperature-dependent resistivity in Ref. [1] without the necessity for invoking any electron-electron scattering.

For completeness, we now directly calculate $\rho(T)$ by treating the disorder scattering exactly at all temperatures by numerically evaluating Eq. (8) and adding the phonon contribution later by hand [see Eq. (18)]. The minimal parameters needed to perform this calculation are the impurity density n_i , the Fermi temperature T_F , the Bloch-Grüneisen temperature T_{BG} , and the electron-phonon coupling λ . Based on qualitative estimates, we choose $n_i = 6 \times 10^{10} \text{ cm}^{-2}$, $T_F = 11 \text{ K}$, $T_{\text{BG}} = 35 \text{ K}$, and $\lambda = 0.05$. We emphasize that these parameters are not obtained by fitting but are estimated based on our analysis of the experimental low- T data (including fitting ρ_0) in the previous section. The resulting numerical $\rho(T)$ is shown in Fig. 4(a) using a logarithmic temperature scale, emphasizing the comparison with the experimental data at low T , as Ref. [1] presented the results on a logarithmic scale. We see that the numerically calculated $\rho(T)$ is consistent with the experimental data. Figure 4(b) shows the same curve in a linear temperature scale, emphasizing the comparison with the experimental data at high T . Here, the numerically calculated $\rho(T)$ is in very good agreement with the experimental data. We emphasize again that our analysis is based on qualitative estimates of the relevant system parameters, and no quantitative predictions can be made at this point because of large uncertainties in the experimental data of Refs. [1,25]. Nevertheless, our result clearly shows that the combination

of disorder and phonon scattering is a plausible explanation for the temperature dependence of the resistivity measured in Ref. [1].

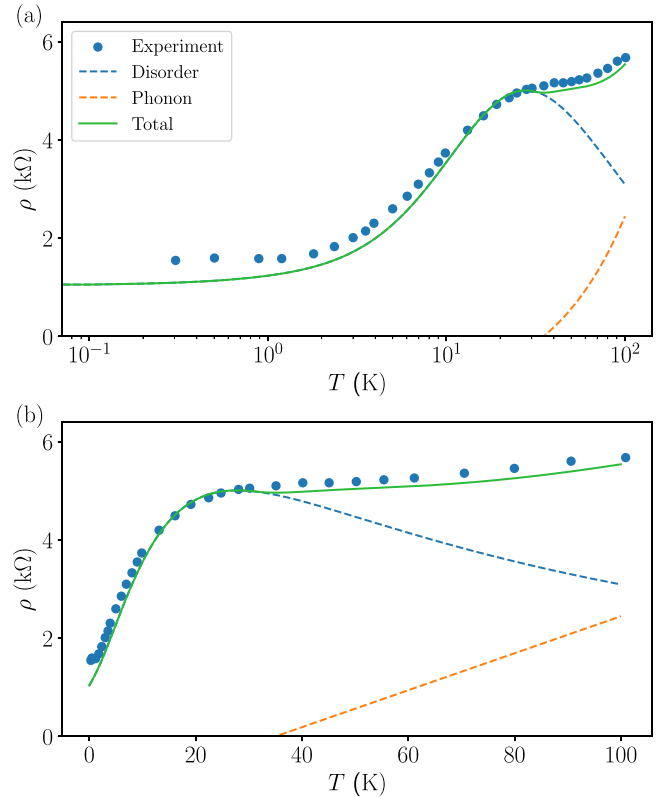


FIG. 4. Contribution to $\rho(T)$ from disorder scattering calculated numerically using Eq. (8) (dashed blue line), empirical phonon resistivity as given in Eq. (18) (dashed orange line), and total resistivity including both disorder scattering and phonon scattering (green line), compared with the experimental resistivity data taken from Ref. [1] at filling $\nu = 1 + 0.35$ (blue dots). The parameters used are $n_i = 6 \times 10^{10} \text{ cm}^{-2}$, $T_F = 11 \text{ K}$, $T_{\text{BG}} = 35 \text{ K}$, and $\lambda = 0.05$. (a) and (b) show the same results, but on a logarithmic temperature scale and a linear temperature scale, respectively.

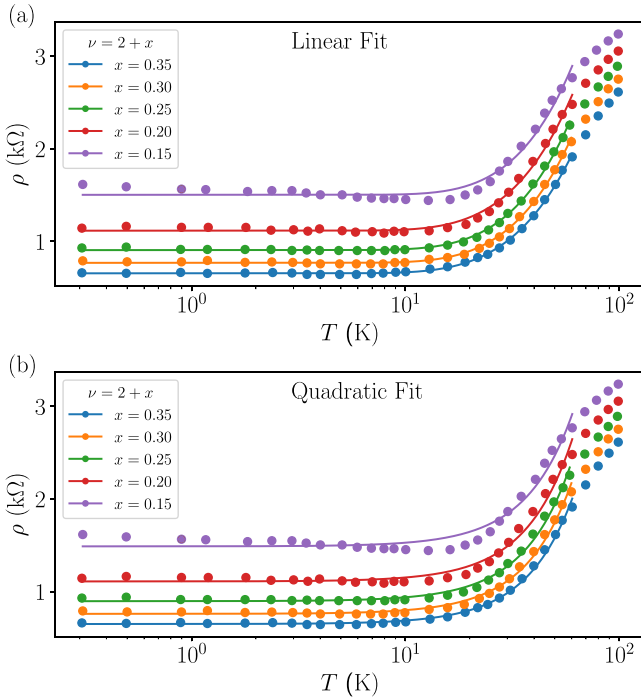


FIG. 5. Fits (solid lines) to the low-temperature experimental resistivity data $\rho(T)$ taken from Ref. [1] (dots) at filling $\nu = 2 + x$. (a) Linear fit (disorder scattering) and (b) quadratic fit (electron-electron scattering). Both fits agree reasonably well with the experimental data.

V. FILLING FACTOR $\nu = 2 + x$

For completeness, we also comment on the low- T behavior of $\rho(T)$ at fillings $\nu = 2 + x$. Again, we perform both a linear and a quadratic fit for $\rho(T)$ at low temperatures in order to compare the importance of electron-electron scattering and disorder scattering. One of the key differences between the resistivity-vs-temperature curves for $\nu = 1 + x$ and $\nu = 2 + x$ is that the latter exhibit an extended low-temperature region where the resistivity is only very weakly temperature dependent. This necessitates the inclusion of a nonzero Dingle temperature in the linear temperature dependence resulting from disorder scattering [see Eq. (11)]. In Fig. 5, we compare a linear fit including a finite Dingle temperature [Fig. 5(a)] and a quadratic fit [Fig. 5(b)] to the experimental resistivity data. Unlike for $\nu = 1 + x$, the quadratic and linear fits perform similarly and are, in fact, hard to distinguish by eye. However, extracting physical quantities from the fit parameters reveals stark differences between the two cases. The linear fit (see Table III) results in values of T_F and m that are of the same order of magnitude as those found for $\nu = 1 + x$. The quadratic fit (electron-electron scattering), on the other hand, gives a significantly larger value of $T_F \sim 200$ K (see Table IV).

VI. CONCLUSIONS

We critically analyzed the temperature dependence of the resistivity presented in Ref. [1], which claims the realization of a Kondo lattice in a Moiré TMD bilayer system.

TABLE III. Fermi temperature T_F , effective mass m , and Dingle temperature T_D as extracted from the linear fit (disorder scattering) to the experimentally reported resistivity of Ref. [1] at filling $\nu = 2 + x$, using $n = xn_M$.

x	T_F (K)	m/m_e	T_D (K)
0.35	30.5	1.6	36.0
0.30	32.0	1.3	38.1
0.25	35.0	1.0	37.8
0.20	41.9	0.7	36.4
0.15	49.5	0.4	43.8

While Ref. [1] inferred the emergence of heavy fermions from the low-temperature resistivity data assuming that electron-electron Fermi liquid scattering is the dominant scattering mechanism, our unbiased comparison of theoretical fits to the experimental data shows that disorder scattering is certainly a viable (if not better) explanation for the resistivity data at low temperatures. Furthermore, at higher temperatures, including a contribution from phonon scattering along with the disorder scattering allowed us to reproduce the experimentally observed resistivity plateau.

For completeness, we mention that there are additional aspects of the experiment that are not explained by our transport calculations, e.g., the reconstruction of the Fermi surface in the presence of a magnetic field. The corresponding experimental Hall conductivity data remain intriguing and would require a high-field generalization of our work. Such a generalization would require understanding the interactions of the local moments in the presence of a magnetic field (including a more realistic band structure) and the corresponding phase transitions that might occur, which is beyond the scope of the current work focusing on explaining the resistivity data at zero magnetic field. While the reported Fermi surface reconstruction is compatible with the Kondo scenario, additional theoretical work would be necessary to conclusively rule out alternative explanations.

In summary, our work shows that a combination of disorder and phonon scattering provides a reasonable alternative explanation for the resistivity data reported in Ref. [1] and that additional experimental signatures are needed to reach a decisive conclusion about whether a Kondo lattice has been observed or not. Given that Ref. [1] reported substantial levels of residual resistivity, impurity scattering is manifestly im-

TABLE IV. Fermi temperature T_F and effective mass m as extracted from the quadratic fit (electron-electron scattering) to the experimentally reported resistivity data of Ref. [1] at filling $\nu = 2 + x$, using $n = xn_M$.

x	T_F (K)	m/m_e
0.35	229.1	0.21
0.30	220.2	0.19
0.25	212.6	0.16
0.20	209.3	0.13
0.15	220.5	0.09

portant, and 2D Fermi surface anomalies automatically lead to a strong temperature dependence in the resistivity arising from the scattering by the Friedel oscillations associated with the quenched charged impurities in the system producing the residual resistivity. Our work is agnostic about the existence of a Kondo lattice in the system studied in Ref. [1] but provides a possible explanation for the temperature-dependent resistivity in terms of disorder and phonon scattering, implying that any Kondo physics, even if it is present, may not affect the

transport properties of the 2D Moiré TMD layers studied in Ref. [1].

ACKNOWLEDGMENTS

We thank K. F. Mak and W. Zhao for helpful discussions on the experimental data and for providing us with unpublished results. This work is supported by the Laboratory for Physical Sciences through the Condensed Matter Theory Center.

-
- [1] W. Zhao, B. Shen, Z. Tao, Z. Han, K. Kang, K. Watanabe, T. Taniguchi, K. F. Mak, and J. Shan, *Nature (London)* **616**, 61 (2023).
- [2] A. Ramires and J. L. Lado, *Phys. Rev. Lett.* **127**, 026401 (2021).
- [3] A. Dalal and J. Ruhman, *Phys. Rev. Res.* **3**, 043173 (2021).
- [4] V. Vaño, M. Amini, S. C. Ganguli, G. Chen, J. L. Lado, S. Kezilebieke, and P. Liljeroth, *Nature (London)* **599**, 582 (2021).
- [5] A. Kumar, N. C. Hu, A. H. MacDonald, and A. C. Potter, *Phys. Rev. B* **106**, L041116 (2022).
- [6] D. Guerci, J. Wang, J. Zang, J. Cano, J. H. Pixley, and A. Millis, *Sci. Adv.* **9**, eade7701 (2023).
- [7] Z.-D. Song and B. A. Bernevig, *Phys. Rev. Lett.* **129**, 047601 (2022).
- [8] Y.-Z. Chou and S. Das Sarma, *Phys. Rev. Lett.* **131**, 026501 (2023).
- [9] H. Hu, B. A. Bernevig, and A. M. Tsvelik, [arXiv:2301.04669](https://arxiv.org/abs/2301.04669).
- [10] H. Hu, G. Rai, L. Crippa, J. Herzog-Arbeitman, D. Călugăru, T. Wehling, G. Sangiovanni, R. Valenti, A. M. Tsvelik, and B. A. Bernevig, [arXiv:2301.04673](https://arxiv.org/abs/2301.04673).
- [11] J. Yu, M. Xie, B. A. Bernevig, and S. Das Sarma, [arXiv:2301.04171](https://arxiv.org/abs/2301.04171).
- [12] V. Mineev, *J. Exp. Theor. Phys.* **132**, 472 (2021).
- [13] P. Coleman, *Many-Body Physics: From Kondo to Hubbard*, edited by E. Pavarini, E. Koch, and P. Coleman (Verlag des Forschungszentrum Jülich, 2015), Vol. 5.
- [14] P. Coleman, C. Pépin, Q. Si, and R. Ramazashvili, *J. Phys.: Condens. Matter* **13**, R723 (2001).
- [15] S. Das Sarma, *Phys. Rev. B* **33**, 5401 (1986).
- [16] S. Das Sarma and E. H. Hwang, *Phys. Rev. Lett.* **83**, 164 (1999).
- [17] S. Das Sarma and E. H. Hwang, *Phys. Rev. B* **68**, 195315 (2003).
- [18] S. Das Sarma and E. H. Hwang, *Phys. Rev. B* **69**, 195305 (2004).
- [19] S. Das Sarma and E. H. Hwang, *Sci. Rep.* **5**, 16655 (2015).
- [20] S. Ahn and S. Das Sarma, *Phys. Rev. B* **106**, L121404 (2022).
- [21] S. Ahn and S. Das Sarma, *Phys. Rev. B* **105**, 115114 (2022).
- [22] H. Min, E. H. Hwang, and S. Das Sarma, *Phys. Rev. B* **86**, 085307 (2012).
- [23] E. H. Hwang and S. Das Sarma, *Phys. Rev. B* **99**, 085105 (2019).
- [24] M. Lavagna, C. Lacroix, and M. Cyrot, *J. Phys. F* **12**, 745 (1982).
- [25] W. Zhao (private communication).
- [26] T. Ando, A. B. Fowler, and F. Stern, *Rev. Mod. Phys.* **54**, 437 (1982).
- [27] F. Stern, *Phys. Rev. Lett.* **18**, 546 (1967).
- [28] A. Gold and V. T. Dolgoplov, *Phys. Rev. B* **33**, 1076 (1986).
- [29] P. F. Maldague, *Surf. Sci.* **73**, 296 (1978).
- [30] G. Zala, B. N. Narozhny, and I. L. Aleiner, *Phys. Rev. B* **64**, 214204 (2001).
- [31] F. Stern, *Phys. Rev. Lett.* **44**, 1469 (1980).
- [32] S. Das Sarma and E. H. Hwang, *Phys. Rev. B* **90**, 035425 (2014).
- [33] L. Zheng and S. Das Sarma, *Phys. Rev. B* **53**, 9964 (1996).
- [34] S. Das Sarma and Y. Liao, *Ann. Phys. (NY)* **435**, 168495 (2021).
- [35] S. Ahn and S. Das Sarma, *Phys. Rev. B* **106**, 155427 (2022).
- [36] K. Behnia, *Ann. Phys. (Berlin, Ger.)* **534**, 2100588 (2022).
- [37] K. Kaasbjerg, K. S. Thygesen, and A.-P. Jauho, *Phys. Rev. B* **87**, 235312 (2013).
- [38] K. Kaasbjerg, T. Low, and A.-P. Jauho, *Phys. Rev. B* **100**, 115409 (2019).
- [39] K. F. Mak (private communication).
- [40] S. Das Sarma and E. H. Hwang, *Phys. Rev. B* **89**, 235423 (2014).